

LETTER TO THE EDITOR

Measuring the hydrostatic mass bias in galaxy clusters by combining Sunyaev-Zel'dovich and CMB lensing data

G. Hurier & R. E. Angulo

Centro de Estudios de Física del Cosmos de Aragón (CEFCA), Plaza de San Juan, 1, planta 2, E-44001, Teruel, Spain.

e-mail: ghurier@cefca.es, rangulo@cefca.es

Preprint online version: July 24, 2018

Abstract

The cosmological parameters preferred by the cosmic microwave background (CMB) primary anisotropies predict many more galaxy clusters than those that have been detected via the thermal Sunyaev-Zel'dovich (tSZ) effect. This tension has attracted considerable attention since it could be evidence of physics beyond the simplest Λ CDM model. However, an accurate and robust calibration of the mass-observable relation for clusters is necessary for the comparison, which has been proven difficult to obtain so far. Here, we present new constraints on the mass-pressure relation by combining tSZ and CMB lensing measurements about optically-selected clusters. Consequently, our galaxy cluster sample is independent from the data employed to derive cosmological constraints. We estimate an average hydrostatic mass bias of $b = 0.26 \pm 0.07$, with no significant mass nor redshift evolution. This value greatly reduces the tension between the predictions of Λ CDM and the observed abundance of tSZ clusters while being in agreement with recent estimations from tSZ clustering. On the other hand, our value for b is higher than the predictions from hydro-dynamical simulations. This suggests the existence of mechanisms driving large departures from hydrostatic equilibrium and that are not included in state-of-the-art simulations, and/or unaccounted systematic errors such as biases in the cluster catalogue due to the optical selection.

Key words. galaxy clusters, CMB, cosmology

1. Introduction

Observations of galaxy clusters via the thermal Sunyaev-Zel'dovich (tSZ) effect, the cosmic microwave background (CMB), and hydrodynamical simulations are in tension: adopting the relation between total mass and gas pressure in clusters predicted by hydrodynamic simulations, the observed abundance of $z < 1$ clusters is considerably lower than what is expected for the Λ CDM parameters preferred by CMB temperature data (Planck Collaboration et al. 2016a, 2014c).

A possible origin for the tSZ-CMB tension is new physics that would modify the growth of structure between the last scattering surface and the present day. However, as shown by Salvati et al. (2017), the tension can not be solved by simple Λ CDM extensions such as massive neutrinos or a time-dependent dark energy equation of state. An alternative explanation is that there are deviations from hydrostatic equilibrium much larger than those predicted by numerical simulations.

Deviations from hydrostatic equilibrium are commonly quantified via the hydrostatic mass bias parameter, b , defined as the fractional difference between the true mass of a cluster and that inferred by a gas proxy assuming hydrostatic equilibrium. Given its importance for cosmology, accurately measuring b and understanding the relevant astrophysics is one of the primary goals in the field of galaxy clusters.

A large number of measurements for b have been performed (e.g., Medezinski et al. 2017; Sereno et al. 2017; Jimeno et al. 2017; Parroni et al. 2017; Okabe & Smith 2016; Battaglia et al. 2016; Applegate et al. 2016; Smith et al. 2016; Hoekstra et al. 2015; Simet et al. 2015; Israel et al. 2015; von der Linden et al. 2014; Donahue et al. 2014; Gruen et al. 2014; Mahdavi et al.

2013). These studies, mostly relying on assumptions of unbiased weak-lensing mass estimates, obtain $b \simeq 0.20 \pm 0.08$. This value is somewhat high compared to that predicted by state-of-the-art hydrodynamical simulations ($b \sim 0.1 - 0.2$, Lau et al. 2013; Hahn et al. 2015; Biffi et al. 2016), but too low to solve the CMB-tSZ tension which would require $b \geq 0.34$ (Salvati et al. 2017). It is noteworthy that a high value of b was preferred by Hurier & Lacasa (2017), who measured $b = 0.30 \pm 0.07$ using a joint analysis of tSZ angular power spectrum, bispectrum, and cluster number-counts.

The above suggests that systematic errors as well as selection biases could perhaps be affecting current estimates of b , or, conversely, that there could be physical processes not captured in current hydrodynamical simulations which would introduce further deviations from hydrostatic equilibrium in clusters. Solving this issue is crucial to derive reliable cosmological constraints and potentially detect deviations from the Λ CDM model.

The recent detection and characterization of the gravitational lensing of CMB photons (Planck Collaboration et al. 2014b), together with all-sky tSZ maps (Planck Collaboration et al. 2016c), have enabled independent and robust constraints on b . CMB lensing has a well-determined source redshift distribution ($z \sim 1100$), which reduces the associated systematic errors.

The correlation between tSZ and CMB lensing potential, ϕ , over the full sky has been measured (Hill & Spergel 2014). Unfortunately, the tSZ- ϕ angular power spectrum does not significantly break the degeneracy between cosmological parameters and b . Additionally, it has been shown that this cross-correlation is significantly contaminated by cosmic infra-red background residuals (CIB, Hurier 2015). In a different approach, Melin & Bartlett (2015) employed the CMB lensing

to measure the individual masses of 61 clusters and derived $b = 0.01 \pm 0.28$. Unfortunately, the low number of systems did not allow these authors to reach high statistical significance.

In the present analysis, we revisit the measurement of the hydrostatic mass bias using CMB lensing and tSZ measurements. We consider galaxy clusters identified by the *red sequence Matched-filter Probabilistic Percolation (redMaPPer)* algorithm (Rykoff et al. 2014) on the SDSS DR8 dataset (Aihara et al. 2011). We measure the stacked tSZ signal about these clusters binned in 4 disjoint richness intervals. We then combine our results with the CMB-lensing measurements of Geach & Peacock (2017), which estimate the total mass for the same clusters. With these two measurements, we place constraints on the cluster hydrostatic mass bias $b = 0.26 \pm 0.07$. Finally, we explore potential redshift or mass dependencies and we discuss the impact of our results on the tSZ-CMB tension.

2. Stacked y signals about redMaPPer clusters

The core of our analysis is to combine the recent CMB weak lensing measurements of Geach & Peacock (2017) with suitable tSZ estimates for the gas pressure in clusters. The CMB weak lensing convergence field is given by $\kappa = \Sigma(R)/\Sigma_{\text{crit}}$, where $\Sigma(R)$ is projected mass density and Σ_{crit} is the critical mass density,

$$\Sigma_{\text{crit}} = \frac{c^2}{4\pi G} \frac{D_{\text{OS}}}{D_{\text{OL}} D_{\text{LS}}}, \quad (1)$$

with D_{OS} , D_{OL} , and D_{LS} the angular diameter distance between the source and the observer, the lens and the observer, and the source and the lens, respectively. For CMB weak lensing, the source is the last scattering surface and the lens is the cluster. Geach & Peacock (2017) used convergence maps built by the Planck satellite to estimate the average total mass, M_{200} , of clusters in the SDSS DR8 redMaPPer clusters catalogue (Rykoff et al. 2014) in four richness bins. We now describe our procedure to estimate the gas pressure for the same clusters.

The intensity of the tSZ signal, y , is proportional to the electronic pressure, P_e , of the intra-cluster medium integrated along the line-of-sight l (Sunyaev & Zeldovich 1972),

$$y = \frac{k_B \sigma_t}{m_e c^2} \int P_e dl. \quad (2)$$

where k_B is the Boltzmann's constant, σ_t is the Thomson's cross section, m_e is the electron rest mass, and c the speed of light. Thus, y maps can be used to estimate P_e and the hydrostatic mass bias when combined with independent cluster mass estimates.

Here, we employ the MILCA y full-sky map (Hurier et al. 2013; Planck Collaboration et al. 2016c) at $7'$ FWHM resolution (previously used in Hurier et al. 2015) in a field of view of 2×2 degrees about each cluster. It is interesting to note that y maps constructed through component separation from multi-frequency data, e.g. MILCA, are biased tracers of the pressure since they neglect relativistic corrections (Wright 1979; Hurier 2016). This induces a significant bias on y (Hurier & Tchernin 2017), but it can be corrected for as we will describe later.

For clusters with significant contamination from radio sources, we re-compute the MILCA map adding extra spectral constraints to reduce the contribution from radio sources (see Hurier et al. 2013, for more details). This procedure significantly increases the noise level, thus, we apply it only to clusters with a clear contamination, as identified in Planck's 70 GHz map.

It is well known that Planck tSZ maps suffer from infrared emission contamination, especially from CIB (Puget et al. 1996). This contamination is particularly important for the tSZ-CMB weak lensing cross correlation power spectrum (Hurier 2015). However, most of this emission originates at high redshift and, by considering the CIB-leakage transfer function in the tSZ MILCA map (Planck Collaboration et al. 2016b), this contamination can be neglected for the stack of our clusters (which are at $z \leq 0.6$).

Following Geach & Peacock (2017), we now stack the tSZ signal about redMaPPer clusters split into four richness, λ , bins: [20,26[, [26,33[, [33,46[, and [46,302]. We note that the tSZ effect and the lensing have different dependencies with the cluster mass and redshift. The lensing signal scales as $M_{500}/\Sigma_{\text{crit}}$, where M_X is the mass contained inside R_X (the radius of a sphere with an average density equal to X times the critical density of the Universe). Whereas, the tSZ flux within a R_{500} aperture, Y_{500} , varies as $M_{500}^{1.79} E(z)^{2/3}$ (Planck Collaboration et al. 2014c).

Therefore, we have weighted the tSZ signal associated to each cluster so that it contributes in the same way as it does to the CMB lensing. Specifically, within a given richness bin we constructed the stacked map, $Y(\theta)$, as:

$$Y(\theta) = \frac{\sum_i w_i y_i}{\sum_i w_i}, \quad w_i = \frac{1}{\lambda_i^{0.79} E(z_i)^{2/3} \Sigma_{\text{crit}}(z_i)}, \quad (3)$$

where y_i is the tSZ MILCA map about the i -th cluster in the richness bin considered. Note that we have assumed that $M_{500} \propto \lambda$. Note also that, if the above dependences are neglected, a combined analysis would have led to significantly biased results ($\approx 50\%$ on b for the [46,302] richness bin).

The final tSZ stacked maps are presented on Fig. 1. Overall, the tSZ signal is detected at 9 and 30σ for the lowest and highest richness bins, respectively.

3. Measurement of the hydrostatic mass bias

The second step in our analysis is to measure the average total tSZ integrated Compton parameter, Y_{TOT} , for each richness bin. We estimate Y_{TOT} as the total Y within an aperture of radius of $10'$ minus the background, estimated in a $10'$ to $30'$ annulus. These two radii are indicated as solid and dashed black circles in Fig. 1. We note that the angular extent of clusters is expected to be smaller than $10'$. Thus, our aperture should capture the whole signal of a cluster. Due to the same reason, our measurement should not be affected by any cluster miscentering.

We estimate the uncertainties in Y_{TOT} using 1000 MILCA maps with different realizations of the instrumental noise (correlated inhomogeneous noise) plus CIB residuals modelled following Planck Collaboration et al. (2016b). We note that the Planck weak-lensing map is constructed using a quadratic estimator of the temperature and polarisation maps (Planck Collaboration et al. 2014b). Hence, the tSZ and lensing maps should have uncorrelated noise and thus we neglect its impact.

We compute the hydrostatic mass bias as the ratio of the cluster mass estimated using our tSZ procedure described above, and the CMB weak lensing masses presented in Geach & Peacock (2017). We convert their mass M_{200} to M_{500} assuming a NFW profile (Navarro et al. 1996) and the mass-concentration relation of Duffy et al. (2008). We transform Y_{TOT} to Y_{500} assuming a gNFW universal pressure profile (Arnaud et al. 2010; Planck Collaboration et al. 2013), which gives $Y_{\text{TOT}}/Y_{500} = 1.79$ (Planck Collaboration et al. 2014a). Finally, we use the scaling relation $Y_{500}-M_{500}$ presented in Planck Collaboration et al.

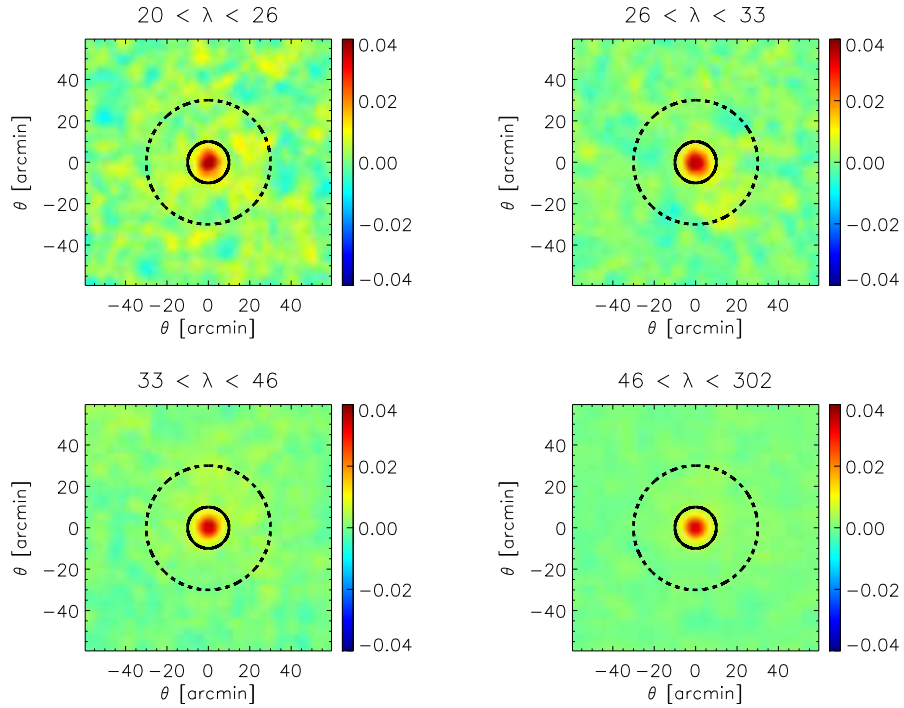


Figure 1. Weighted stacking of the Planck tSZ MILCA map at 7' FWHM for a field of view of 2x2 degrees for four richness, λ , bins. The stacked tSZ signal is shown in arbitrary units. The solid line black line delimits the region used to estimated the total tSZ flux, Y_{TOT} and the dashed black line delimits the region used to estimate the zero-level of the tSZ stack maps.

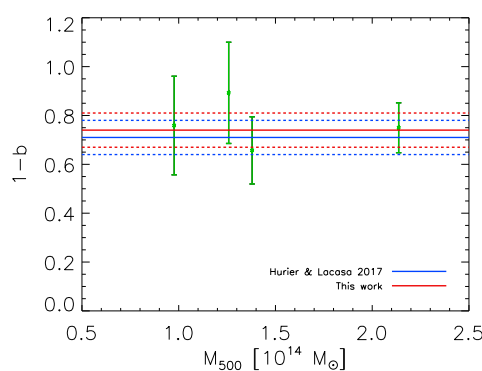


Figure 2. Measurement of the hydrostatic mass bias derived from Planck tSZ and Planck CMB weak lensing data (green symbols). The best fitting average bias is shown as a red solid line, dashed red lines shows the 1- σ uncertainty level. For comparison, we also display the constraints from Hurier & Lacasa (2017) as blue lines.

(2014c) to compute the cluster mass. This relation assumes hydrostatic equilibrium and has been calibrated on Planck data and X-ray observations (note, however, that this relation does not include relativistic corrections and, consequently, in the previous section we used uncorrected y maps).

We present the resulting values for the hydrostatic mass bias in Fig. 2. Error bars include the uncertainty associated to both tSZ and CMB-lensing mass estimates. We derived an average bias of $b = 0.26 \pm 0.07$. This value is consistent within 1- σ with

previous analyses performed on CMB weak lensing (Melin & Bartlett 2015), and gives slightly higher but consistent results with previous galaxy-galaxy weak-lensing based analyses (see e.g., Medezinski et al. 2017; Sereno et al. 2017; Jimeno et al. 2017; Parroni et al. 2017; Okabe & Smith 2016; Battaglia et al. 2016; Applegate et al. 2016; Smith et al. 2016; Hoekstra et al. 2015; Simet et al. 2015; Israel et al. 2015; von der Linden et al. 2014; Donahue et al. 2014; Gruen et al. 2014; Mahdavi et al. 2013). This value for b is also consistent with previous results obtained from the tSZ analysis performed in Hurier & Lacasa (2017) but it favours slightly lower values than the combined analysis of CMB and tSZ performed by Salvati et al. (2017).

We fitted for an eventual mass or redshift evolution of the hydrostatic mass bias. First we assumed the following expression,

$$b = b_0 + b_1 \left(\frac{M_{500} - 10^{14} [M_\odot]}{10^{15} [M_\odot]} \right). \quad (4)$$

We derived, $b_0 = 0.26 \pm 0.13$ and $b_1 = -0.02 \pm 1.50$, consistent with no mass evolution for the bias. Then we considered,

$$b = b_2 \left(\frac{1+z}{1.38} \right)^\alpha. \quad (5)$$

We derived, $b_2 = 0.26 \pm 0.08$ and $\alpha = 0.30 \pm 0.37$, consistent within 1- σ with no redshift evolution for the hydrostatic mass bias. Given that we do not observe significant mass or redshift dependencies, we expect our results to not be significantly affected by selection effects of the *redMaPPer* cluster sample in the mass-redshift plane.

4. Conclusion and discussion

We have performed a combined analysis of tSZ and CMB weak lensing effects about SDSS DR8 redMaPPer clusters. The CMB weak lensing only depends on the integrated amount of matter along the line-of-sight. Thus it offers the opportunity to calibrate scaling relations related to baryonic physics with a high accuracy and little to no systematic effects.

We have inferred a value for the hydrostatic mass bias $b = 0.26 \pm 0.07$ with no significant redshift or mass evolution. However, the significantly different constraints derived previously from tSZ and tSZ-X-ray cross-correlation (Hurier et al. 2015; Hurier & Lacasa 2017) may indicate that high-mass, low- z clusters tend to be slightly less-biased. In addition, the uncertainty in our value (mostly due to the uncertainty in CMB lensing mass estimates) prevents us from conclusive statements about whether clusters can be modelled with a single b value or not. Nevertheless, our value for b does have implications for the tSZ-CMB tension, as we will see next.

In Fig. 3 we show several cosmological constraints for $\Sigma_8 = \sigma_8 (\Omega_m/0.30)^{0.27}$ updated by adopting our new estimate for the hydrostatic mass bias. Specifically, we obtain: $\Sigma_8 = 0.75 \pm 0.03$ for the tSZ analysis presented in Hurier & Lacasa (2017), $\Sigma_8 = 0.79 \pm 0.04$ for the tSZ-CMB weak lensing cross-correlation (Hurier 2015), and $\Sigma_8 = 0.83 \pm 0.05$ for the X-ray-tSZ cross-correlation (Hurier et al. 2015). For comparison, we also show the constraints assuming instead $b = 0.20 \pm 0.05$ – a value favoured by hydrodynamical simulations.

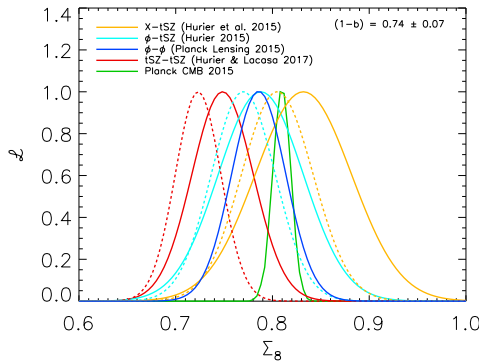


Figure 3. Likelihood distribution of $\Sigma_8 = \sigma_8 (\Omega_m/0.30)^{0.27}$ for different analyses: tSZ angular power spectrum, bispectrum, and number count (red, Hurier & Lacasa 2017), CMB weak lensing (dark blue, Planck Collaboration et al. 2014b), CMB angular power spectrum (green, Planck Collaboration et al. 2016a), tSZ-weak lensing cross correlation (light blue, Hurier 2015), and tSZ-X-ray cross-correlation (orange, Hurier et al. 2015). The dashed lines shows the same likelihood functions assuming $b = 0.2 \pm 0.05$ whereas the solid lines uses our measured value $b = 0.26 \pm 0.07$.

Our constraints bracket the expected value from CMB angular power spectrum analysis, $\Sigma_8 = 0.81 \pm 0.01$, and are also consistent with the CMB weak-lensing analysis (green and blue lines in Fig. 3, respectively). In fact, all the cluster- and CMB-based constraints agree within 2σ , reducing the tension between the cluster abundances and the CMB. Thus suggests that the structure in the local and early Universe are fully consistent within the simplest Λ CDM model.

Conversely, our results are now in clear tension with cluster hydrodynamical simulations that predict low values for the hydrostatic mass bias, $b < 0.2$. This would imply the lack of important physical processes in current simulations or large unaccounted systematic errors in observations (e.g. selection biases in the optical cluster catalogue). In the future, more sophisticated simulations with realistic mock observations as well as more accurate CMB-lensing measurements will shed light on the origin of this discrepancy.

Acknowledgement

We acknowledge the use of HEALPix (Górski et al. 2005). This project has received funding from the Spanish Ministerio de Economía and Competitividad (MINECO) through grant number AYA2015-66211-C2-2. REA acknowledges support of the European Research Council through grant number ERC-StG/716151.

References

Aihara, H., Allende Prieto, C., An, D., et al. 2011, ApJS, 193, 29
 Applegate, D. E., Mantz, A., Allen, S. W., et al. 2016, MNRAS, 457, 1522
 Arnaud, M., Pratt, G. W., Piffaretti, R., et al. 2010, A&A, 517, A92
 Battaglia, N., Leauthaud, A., Miyatake, H., et al. 2016, J. Cosmology Astropart. Phys., 8, 013
 Biffi, V., Borgani, S., Murante, G., et al. 2016, ApJ, 827, 112
 Donahue, M., Voit, G. M., Mahdavi, A., et al. 2014, ApJ, 794, 136
 Duffy, A. R., Schaye, J., Kay, S. T., & Dalla Vecchia, C. 2008, MNRAS, 390, L64
 Geach, J. E. & Peacock, J. A. 2017, ArXiv e-prints
 Górski, K. M., Hivon, E., Banday, A. J., et al. 2005, ApJ, 622, 759
 Gruen, D., Seitz, S., Brimiouille, F., et al. 2014, MNRAS, 442, 1507
 Hahn, O., Martizzi, D., Wu, H.-Y., et al. 2015, ArXiv e-prints
 Hill, J. C. & Spergel, D. N. 2014, J. Cosmology Astropart. Phys., 2, 030
 Hoekstra, H., Herbonnet, R., Muzzin, A., et al. 2015, MNRAS, 449, 685
 Hurier, G. 2015, A&A, 575, L11
 Hurier, G. 2016, A&A, 596, A61
 Hurier, G., Douspis, M., Aghanim, N., et al. 2015, A&A, 576, A90
 Hurier, G. & Lacasa, F. 2017, ArXiv e-prints
 Hurier, G., Macías-Pérez, J. F., & Hildebrandt, S. 2013, A&A, 558, A118
 Hurier, G. & Tchernin, C. 2017, ArXiv e-prints
 Israel, H., Schellenberger, G., Nevalainen, J., Massey, R., & Reiprich, T. H. 2015, MNRAS, 448, 814
 Jimeno, P., Diego, J.-M., Broadhurst, T., De Martino, I., & Lazkoz, R. 2017, ArXiv e-prints
 Lau, E. T., Nagai, D., & Nelson, K. 2013, ApJ, 777, 151
 Mahdavi, A., Hoekstra, H., Babul, A., et al. 2013, ApJ, 767, 116
 Medezinski, E., Battaglia, N., Umetsu, K., et al. 2017, ArXiv e-prints
 Melin, J.-B. & Bartlett, J. G. 2015, A&A, 578, A21
 Navarro, J. F., Frenk, C. S., & White, S. D. M. 1996, ApJ, 462, 563
 Okabe, N. & Smith, G. P. 2016, MNRAS, 461, 3794
 Parroni, C., Mei, S., Erben, T., et al. 2017, ArXiv e-prints
 Planck Collaboration, Ade, P. A. R., Aghanim, N., et al. 2014a, A&A, 571, A29
 Planck Collaboration, Ade, P. A. R., Aghanim, N., et al. 2014b, A&A, 571, A17
 Planck Collaboration, Ade, P. A. R., Aghanim, N., et al. 2014c, A&A, 571, A20
 Planck Collaboration, Ade, P. A. R., Aghanim, N., et al. 2013, A&A, 550, A131
 Planck Collaboration, Ade, P. A. R., Aghanim, N., et al. 2016a, A&A, 594, A13
 Planck Collaboration, Ade, P. A. R., Aghanim, N., et al. 2016b, A&A, 594, A23
 Planck Collaboration, Aghanim, N., Arnaud, M., et al. 2016c, A&A, 594, A22
 Puget, J.-L., Abergel, A., Bernard, J.-P., et al. 1996, A&A, 308, L5
 Rykoff, E. S., Rozo, E., Busha, M. T., et al. 2014, ApJ, 785, 104
 Salvati, L., Douspis, M., & Aghanim, N. 2017, ArXiv e-prints
 Sereno, M., Covone, G., Izzo, L., et al. 2017, ArXiv e-prints
 Simet, M., Battaglia, N., Mandelbaum, R., & Seljak, U. 2015, in American Astronomical Society Meeting Abstracts, Vol. 225, American Astronomical Society Meeting Abstracts, 443.04
 Smith, G. P., Mazzotta, P., Okabe, N., et al. 2016, MNRAS, 456, L74
 Sunyaev, R. A. & Zeldovich, Y. B. 1972, Comments on Astrophysics and Space Physics, 4, 173
 von der Linden, A., Mantz, A., Allen, S. W., et al. 2014, MNRAS, 443, 1973
 Wright, E. L. 1979, ApJ, 232, 348